

Exact Hidden Markovian Dynamics in Quantum Circuits

He-Ran Wang,¹ Xiao-Yang Yang,^{1,2} and Zhong Wang^{1,*}

¹*Institute for Advanced Study, Tsinghua University, Beijing 100084, People's Republic of China*

²*Department of Physics, Tsinghua University, Beijing 100084, People's Republic of China*

Characterizing nonequilibrium dynamics in quantum many-body systems is a challenging frontier of physics. In this Letter, we systematically construct solvable nonintegrable quantum circuits that exhibit exact hidden Markovian subsystem dynamics. This feature thus enables accurately calculating local observables for arbitrary evolution time. Utilizing the influence matrix method, we show that the influence of the time-evolved global system on a finite subsystem can be analytically described by sequential, time-local quantum channels acting on the subsystem with an ancilla of finite Hilbert space dimension. The realization of exact hidden Markovian property is facilitated by a solvable condition on the underlying two-site gates in the quantum circuit. We further present several concrete examples with varying local Hilbert space dimensions to demonstrate our approach.

In isolated quantum many-body systems driven out of equilibrium, thermalization typically occurs, where local observables relax to their thermal-averaged expectation values after a finite time. Heuristically, the global system serves as a thermal bath for the local subsystem [1–6]. On the other hand, various counterexamples of thermalization have been extensively studied, including integrable models [7], many-body localization [8, 9], and quantum many-body scars [10–12]. However, for both scenarios (following or violating thermalization), it poses a formidable challenge to accurately quantify the influence of the time-evolved macroscopic many-body system on its own subsystem, due to the exponentially large Hilbert space dimension in the thermodynamic limit and the quantum memory effects brought by the non-Markovianity.

Recently, progress has been made in quantum circuits, where the unitary evolution is discretized to sequences of local unitary gates. In particular, Refs. [13–19] have developed an efficient tensor-network approach to trace out the system, and encode the influence on the subsystem into the fixed point of the spatial transfer matrix, which is also known as the *influence matrix* [17, 18]. However, the intrinsic complexity of many-body dynamics typically leads to complicated influence matrices as the evolution time grows, restricting rigorous numerical and analytical treatment within this approach [20].

Here, we introduce a novel approach to systematically constructing 1+1 D nonintegrable quantum circuits exhibiting exact hidden Markovian subsystem dynamics. We introduce a solvable condition for the underlying unitary gates allowing for efficient contractions of quantum-circuit tensor networks for arbitrary evolution time. We show that the time-evolved system can be traced out to a closed-form influence matrix in the matrix product state (MPS) representation of finite bond dimension for arbitrary evolution time, thus enabling numerical calculations of subsystem dynamics in an exact fashion. Notably, we interpret the influence matrix as sequential quantum channels acting on the subsystem boundary. Hence, our work uncovers new principles leading to subsystem hidden Markovian property, and provides a promising testground to explore rich phenomena in quantum many-body dynamics through analytical tools.

The setup—In this letter we consider quantum circuits on a 1D lattice, where each site is labeled by an integer x . We

associate a q -dimensional Hilbert space \mathcal{H}_q for each site, with a basis: $\{|a\rangle, a = 0, 1, \dots, q-1\}$. The system is prepared in the initial state $|\Psi_{\text{in}}\rangle$ and undergoes discrete time evolution. For each time step, the global unitary operator is $\mathbb{U} = \mathbb{U}_{\text{odd}}\mathbb{U}_{\text{even}}$, where $\mathbb{U}_{\text{odd}(\text{even})} = \otimes_{x \in \text{odd}(\text{even})} U_{x,x+1}$. $U_{x,x+1}$ are two-site gates acting locally on x and $x+1$. As indicated by the form of \mathbb{U} , the local gates are arranged in a brickwork architecture.

For the sake of convenience in depiction, we fold the forward and backward branches of time evolution [see Fig. 1(a)]. By folding, each tensor is superimposed on its complex conjugate. The folded two-site unitary gate acting on the doubled space is defined as the following four-leg tensor:

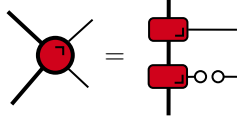
$$\begin{array}{c} c, c' \\ \diagdown \quad \diagup \\ \text{---} \square \text{---} \\ \diagup \quad \diagdown \\ a, a' \quad b, b' \end{array} = U_{ab}^{cd} \left(U_{a'b'}^{c'd'} \right)^*, \quad (1)$$

where a, b, c, d (a', b', c', d') denote the basis states in the forward (backward) branch.

We focus on a certain class of initial states on the composite system L - R , with L (R) for the left (right), as shown in Fig. 1(b). For later convenience, we set the location of the leftmost site on R as the origin point $x = 0$. The global unitary operator admits a decomposition as $\mathbb{U} = \mathbb{U}_{\bar{R}}\mathbb{U}_R$, where \mathbb{U}_R acts nontrivially on R , and $\mathbb{U}_{\bar{R}}$ acts on L and the boundary across the two regions. Meanwhile, we assume that the overall initial state can be decomposed as $|\Psi_{\text{in}}\rangle = \sum_{j=1}^{\chi} |\Psi_L^j\rangle \otimes |\Psi_R^j\rangle$ (where each $|\Psi_{R/L}^j\rangle$ is not required to be normalized). Here, we consider generic $|\Psi_R^j\rangle$ on the right, while $|\Psi_L^j\rangle$ can be written as a one-site shift-invariant MPS of bond dimension χ in terms of the three-leg tensor $A_{jk}^{(a)}$, where $j = 0, 1, \dots, \chi-1$. The matrices $\{A^{(a)}\}$ act on the auxiliary Hilbert space \mathcal{H}_{χ} spanned by the basis $\{|j\rangle\}_{j=0}^{\chi-1}$. Graphically, we can represent the folded tensor A as

$$\begin{array}{c} a, a' \\ | \\ j, j' \text{---} \square \text{---} k, k' \end{array} = A_{jk}^{(a)} A_{j'k'}^{(a')*}, \quad (2)$$

MPS of bond dimension χ^2 with appropriate boundary conditions. The replicated element in the MPS is the following four-leg tensor:



$$(5)$$

This local tensor can be represented explicitly in terms of A [38], and replicates T times in the IM. At the lower boundary $t = 0$, the auxiliary leg is connected to the initial state in the region R ; at the upper boundary $t = T$, the auxiliary Hilbert space is traced out. Interestingly, the form of the IM indicates the nonsignaling property of the subsystem dynamics [39–42]: the information flowing from the subsystem to the environment is completely discarded, as implied by the trace operator in Eq. (5), and can never flow back into the subsystem. However, the environment retains the memory of initial correlations between L and R .

Exact hidden Markovian subsystem dynamics—Next, we show that the exact IM gives rise to hidden Markovian dynamics of the subsystem. As implied by the MPS representation, the IM is correlated in the time direction (when $\chi > 1$), and thus the Markovian property is lacking [24, 25, 43, 44]. Nevertheless, we can incorporate an ancilla of *finite dimension* into the subsystem, which renders the joint dynamics to be governed by sequential quantum channels. The ancilla lives in the auxiliary Hilbert space \mathcal{H}_χ . We term such dynamics as *hidden Markovian*, aligning with its classical counterpart [45–47]. At $t = 0$, we prepare the joint system in the pure state as $|\tilde{\Psi}_R\rangle = \sum_{j=0}^{\chi-1} |j\rangle \otimes |\Psi_R^j\rangle$, which gives the same subsystem reduced density matrix when tracing out the ancilla. Here, \otimes denotes tensor products between the auxiliary and physical Hilbert space. Hence, the initial correlations between two regions are captured by this ancilla. As illustrated in Fig. 1(d), for each time step, the joint system is evolved by a layer of local gates, followed by a two-site quantum channel \mathcal{M} acting on the ancilla and the leftmost site,

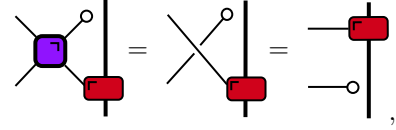
$$\tilde{\rho}_R(t+1) = \mathcal{M}[\mathbb{U}_R \tilde{\rho}_R(t) \mathbb{U}_R^\dagger], \quad (6)$$

where $\tilde{\rho}_R(t)$ is the joint system density matrix at time t . The dynamics of $\tilde{\rho}_R(t)$ is explicitly Markovian [48], where the state at the $(t+1)$ th time step only depends on the state at t . The quantum channel \mathcal{M} is given by the four-leg tensor defined in Eq. (5), which can be written in the standard Kraus form [38, 49], $\mathcal{M}(\tilde{\rho}_R) = \sum_\mu K_\mu \tilde{\rho}_R K_\mu^\dagger$, where

$$K_\mu = K_{a,a'} = \sum_{b=0}^{q-1} A^{(b)} A^{(a)} \otimes (|b\rangle \langle a'|)_{x=0}. \quad (7)$$

Here a, a' run over 0 to $q-1$. Provided the Kraus-form representation, the quantum channel \mathcal{M} is completely positive and trace-preserving [50]. The reduced density matrix on R can be obtained by tracing out the ancilla at each time step: $\rho_R(t) = \text{Tr}_{\mathcal{H}_\chi}[\tilde{\rho}_R(t)]$.

A few remarks are in order. First, we can prepare the left initial state in a matrix product density operator, instead of a MPS pure state. All the analysis works as well, except that the expression of Kraus form should be slightly modified [38]. Second, the left initial states can be extended to a certain class of two-site shift-invariant MPS, while keeping the solvability of the influence matrix [38]. Third, due to the chiral structure in the solvable condition, it only allows efficient contractions of tensor networks from left to right, but not vice versa. However, by imposing an additional condition as follows,



$$(8)$$

contractions from the right are allowed as well (see [38] for concrete examples). Quantum circuits equipped with two solvable conditions of opposite chirality facilitate analytical descriptions for more physical quantities, e.g., Rényi entropy dynamics [51]. Specifically, in [38] we show that the n th entanglement velocity $v_E^{(n)}$ [52] – the asymptotic growing rate of the n th Rényi entropy ($n > 1$) between two regions – is given by the leading eigenvalue λ_n of a certain quantum channel,

$$v_E^{(n)} \equiv \lim_{t \rightarrow \infty} \frac{\ln(\text{Tr}[\rho_R^n(t)]) / (1-n)}{t \ln(q)} = \frac{2 \ln(\lambda_n)}{(1-n) \ln(q)}. \quad (9)$$

The entanglement velocity explicitly depends on the Rényi index n , which is clearly different from dual-unitary gates with solvable initial state [27].

Next, we demonstrate that solutions (up to one-site unitaries) of Eq. (4) actually depend only on two characteristic values, q and \tilde{q} , of the local tensor $A_{jk}^{(a)}$, rather than on exact values of all the tensor elements. Here, q is the local Hilbert space dimension, and \tilde{q} is the one-site MPS dimension which will be clarified later. For convenience, we define the reshuffled operator U^R as $(U^R)_{ab}^{cd} = U^{bd}_{ac}$. When read along the space direction, the solvable condition can be expressed as

$$U^R(|A_{jk}\rangle \langle A_{j'k'}| \otimes I_q)(U^R)^\dagger = I_q \otimes |A_{jk}\rangle \langle A_{j'k'}|, \quad (10)$$

for all combinations of j, j', k, k' . Here, I_q is the identity operator in the local Hilbert space, and the one-site MPS is defined as $|A_{jk}\rangle = \sum_{a=0}^{q-1} A_{jk}^{(a)} |a\rangle$. This expression suggests that the set of solutions U essentially depends on the Hilbert subspace \mathcal{H}_A spanned by $\{|A_{jk}\rangle\}_{j,k=1}^X$. Furthermore, due to the isomorphism between different Hilbert subspaces with the same dimension, the solutions should solely rely on the subspace dimension $\tilde{q} = \dim(\mathcal{H}_A)$, up to one-site unitaries.

Since the set of solutions applies to all initial states with the same q and \tilde{q} , we will label the solutions by these two characteristic values in the following.

Example 1—In this and the next part, we will show that the solvable condition indeed leads to a wide range of solutions for quantum circuits. First, we present the solutions of $q = 2, \tilde{q} = 1$. For the reason demonstrated above, we can

take a specific left initial state $\otimes_{x<0} |0\rangle_x$. In the context of MPS, the tensors are given by $A^{(0)} = 1, A^{(1)} = 0$, and thus $\mathcal{H}_A = \{|0\rangle\}$. We provide an exhaustive parametrization for the solutions [38]

$$U = e^{i\phi}(u \otimes e^{-i\epsilon\sigma^3})V[J](e^{-i\eta\sigma^3} \otimes v), \quad (11)$$

where $u, v \in \text{SU}(2)$, and

$$V[J] = \exp[-i(\frac{\pi}{4}\sigma^1 \otimes \sigma^1 + \frac{\pi}{4}\sigma^2 \otimes \sigma^2 + J\sigma^3 \otimes \sigma^3)].$$

Here, σ^α , $\alpha = 1, 2, 3$ are standard Pauli matrices. This class of solutions coincides with those two-qubit circuits featured in chiral solitons, which are dual unitary [53].

Compared to those previously known solvable initial states for dual-unitary circuits [26], our findings suggest a new initial state $(\otimes_{x<0} |0\rangle_x)$ allowing for exact influence matrix in the product-state form. The corresponding one-site quantum channel can be obtained by substituting the form of A into Eq. (7): $\mathcal{M}[\rho_R] = (|0\rangle\langle 0|)_{x=0} \otimes \text{Tr}_{x=0}[\rho_R]$. Hence, the left bath acts as the boundary resetting toward $|0\rangle$, and thus the entanglement between two regions never grows up. In addition, we point out that for the solutions Eq. (11), we can independently choose the one-site initial state as $|0\rangle$ or $|1\rangle$ while holding the solvability of the influence matrix.

Example II—Next, we present a (nonexhaustive) parametrization for solutions with $q = 4, \tilde{q} = 2$, where \mathcal{H}_A is spanned by $|0\rangle$ and $|1\rangle$,

$$U = e^{i\phi}W_2SW_1(I \otimes v). \quad (12)$$

Here, $v \in \text{SU}(4)$, S is the SWAP gate, $W_{1,2}$ are one-site controlled gates,

$$W_{1,2} = \sum_{a=0}^3 f_{1,2}^{(a)} \otimes |a\rangle\langle a|, \quad (13)$$

where $f_1^{(a)} = \begin{pmatrix} I_2 & 0 \\ 0 & g^{(a)} \end{pmatrix}$, $g^{(a)} \in \text{SU}(2)$, and $f_2^{(a)} \in \text{SU}(4)$ for all a . The parametrization can be generalized to higher q and \tilde{q} with slight modifications: $v \in \text{SU}(q)$, $f_1^{(a)} = I_{\tilde{q}} \oplus g^{(a)}$, where $g^{(a)} \in \text{SU}(q - \tilde{q})$, and $f_2^{(a)} \in \text{SU}(q)$. Generally, these solutions form an overlapping but different set with dual-unitary circuits. An exception is when $q - \tilde{q} = 0$ or 1 , where $f_1^{(a)} = I_q, W_1 = I_{q^2}$ and thus Eq. (12) is reduced to a subclass of dual-unitary gates [54, 55].

As an illustrative example, we report numerical results about the finite-size subsystem entanglement dynamics evolved by Eq. (12). For the left initial state, we choose the following $\chi = 2$ MPS, which spans \mathcal{H}_A with $\tilde{q} = 2$: $A^{(0)} = \begin{pmatrix} \cos(\theta) & \sin(\theta) \\ 0 & 0 \end{pmatrix}$, $A^{(1)} = \begin{pmatrix} 0 & 0 \\ -\sin(\theta) & \cos(\theta) \end{pmatrix}$, and $A^{(2,3)} = 0$. Here $\theta \in (0, \frac{\pi}{4}]$, which corresponds to the left initial state interpolating between the Greenberger-Horne-Zeilinger state and the cluster state [56, 57] of basis states $|0\rangle$ and $|1\rangle$. As for the right region, we take the initial state as the

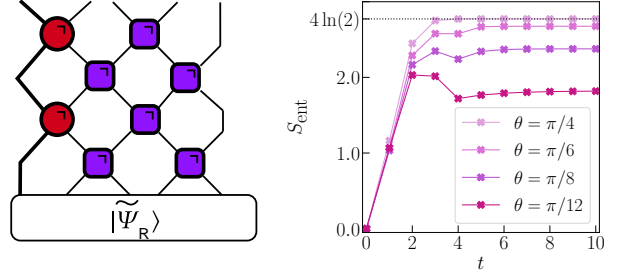


FIG. 2. Entanglement dynamics. Left panel: illustration of the joint system, where the right region consists of four sites. Right panel: Growth of subsystem von Neumann entropies for different left initial MPSs, which are characterized by the value of θ . The right initial state and two-site gates are kept the same. The horizontal dotted line marks the maximal entropy $4 \ln(2)$ approached by $\theta = \pi/4$.

simple product state $|\Psi_R^j\rangle = \otimes_{x \geq 0} |2\rangle_x$, $j = 0, 1$, and thus the initial entanglement between regions L and R is zero. The right subsystem consists of four sites as shown faithfully in the left panel of Fig. 2. We construct the two-site gate U by randomly generating unitaries $v, g^{(a)}$, and $f_2^{(a)}$.

Employing the influence matrix method, we can numerically keep track of the full time evolution of the joint system. The joint dynamics is generated by the Floquet operator Eq. (6), which is constituted by the unitary \mathbb{U}_R along with the boundary quantum channel \mathcal{M} given by Eq. (7). We compute the von Neumann entanglement entropy between two regions as $S_{\text{ent}}(t) = -\text{Tr}\{\rho_R(t) \ln[\rho_R(t)]\}$. We emphasize that the scenario here is basically different from that described by Eq. (9), where the size of R is infinitely large. Results for various values of θ are depicted in the right panel of Fig. 2. Following a similar rate of linear growth in the early stage of evolution, the entropies approach the θ -dependent steady values after finite time steps. Among the steady values, the maximal entropy $4 \ln(2)$ is achieved by the case $\theta = \pi/4$, corresponding to the cluster state as the initial MPS. Notably, this maximal saturated entropy is still smaller than the maximum entropy allowed by the Hilbert space dimension of the right subsystem $\ln(q^{L_R}) = 4 \ln(4)$, which suggests violating the thermalization toward an infinite-temperature state. This observation hints at the existence of hidden conservation quantities, which demands further research.

Conclusions—In summary, we have established a systematic approach toward construction of nonintegrable quantum circuits exhibiting exact hidden Markovian subsystem dynamics. We introduced new principles beyond dual-unitary circuits allowing for closed-form influence matrices of finite bond dimension, which are formulated into the solvable condition on local unitary gates. Utilizing the tensor-network method, we demonstrated that the system acts as time-local boundary quantum channels on the subsystem, thus inducing exact hidden Markovian dynamics. Our constructions have unveiled a novel spacetime duality between the initial state MPS of the system and boundary quantum channels acting on

the reduced subsystem.

Our work opens up many avenues for future research, such as the introduction of measurements [58] and dissipation [59], and generalizations to different architectures [55, 60] and higher spatial dimensions [28, 61, 62]. The exact influence matrices also provide valuable analytical tools for studying rich phenomena in quantum many-body dynamics, including quantum chaos [63], scrambling [64], and deep thermalization [58, 65, 66].

Furthermore, our findings on the exact hidden Markovian property could provide fresh insights into the fundamental understanding of the Markovian approximation. A valid Markovian approximation often resorts to weak system-bath coupling and the separation of timescales [67, 68]. However, in a quantum many-body system, focusing on a subsystem and integrating out the rest usually yields non-Markovian subsystem dynamics, because the “bath” and the subsystem typically undergo the same type of dynamics and thus the corresponding timescales are comparable [69]. In contrast, in our construction the Markovian property emerges nonperturbatively as a consequence of the solvable condition, even provided the presence of initial genuine quantum correlations between the subsystem and the bath. Understanding deep relations between these solvable quantum circuits and the Markovian approximation remains an intriguing area for further exploration.

Acknowledgments—We thank Tianci Zhou for helpful discussions. This work was supported by the National Natural Science Foundation of China (Grant No. 12125405), and National Key R&D Program of China (No. 2023YFA1406702).

* wangzhongemail@tsinghua.edu.cn

- [1] J. M. Deutsch, “Quantum statistical mechanics in a closed system,” *Phys. Rev. A* **43**, 2046 (1991).
- [2] M. Srednicki, “Chaos and quantum thermalization,” *Phys. Rev. E* **50**, 888 (1994).
- [3] M. Rigol, V. Dunjko, and M. Olshanii, “Thermalization and its mechanism for generic isolated quantum systems,” *Nature* **452**, 854 (2008).
- [4] M. A. Cazalilla and M. Rigol, “Focus on dynamics and thermalization in isolated quantum many-body systems,” *New J. Phys.* **12**, 055006 (2010).
- [5] A. Polkovnikov, K. Sengupta, A. Silva, and M. Vengalattore, “Colloquium: Nonequilibrium dynamics of closed interacting quantum systems,” *Rev. Mod. Phys.* **83**, 863 (2011).
- [6] R. Kosloff, “Quantum thermodynamics: A dynamical viewpoint,” *Entropy* **15**, 2100 (2013).
- [7] B. Sutherland, *Beautiful models: 70 years of exactly solved quantum many-body problems* (World Scientific, 2004).
- [8] R. Nandkishore and D. A. Huse, “Many-body localization and thermalization in quantum statistical mechanics,” *Annu. Rev. Condens. Matter Phys.* **6**, 15 (2015).
- [9] D. A. Abanin, E. Altman, I. Bloch, and M. Serbyn, “Colloquium: Many-body localization, thermalization, and entanglement,” *Rev. Mod. Phys.* **91**, 021001 (2019).
- [10] M. Serbyn, D. A. Abanin, and Z. Papić, “Quantum many-body scars and weak breaking of ergodicity,” *Nat. Phys.* **17**, 675 (2021).
- [11] S. Moudgalya, B. A. Bernevig, and N. Regnault, “Quantum many-body scars and hilbert space fragmentation: A review of exact results,” *Rep. Prog. Phys.* **85**, 086501 (2022).
- [12] A. Chandran, T. Iadecola, V. Khemani, and R. Moessner, “Quantum many-body scars: A quasiparticle perspective,” *Annu. Rev. Condens. Matter Phys.* **14** (2022).
- [13] M. C. Bañuls, M. B. Hastings, F. Verstraete, and J. I. Cirac, “Matrix product states for dynamical simulation of infinite chains,” *Phys. Rev. Lett.* **102**, 240603 (2009).
- [14] A. Müller-Hermes, J. I. Cirac, and M. C. Bañuls, “Tensor network techniques for the computation of dynamical observables in one-dimensional quantum spin systems,” *New J. Phys.* **14**, 075003 (2012).
- [15] M. B. Hastings and R. Mahajan, “Connecting entanglement in time and space: Improving the folding algorithm,” *Phys. Rev. A* **91**, 032306 (2015).
- [16] M. Frías-Pérez and M. C. Bañuls, “Light cone tensor network and time evolution,” *Phys. Rev. B* **106**, 115117 (2022).
- [17] A. Lerose, M. Sonner, and D. A. Abanin, “Influence matrix approach to many-body floquet dynamics,” *Phys. Rev. X* **11**, 021040 (2021).
- [18] M. Sonner, A. Lerose, and D. A. Abanin, “Influence functional of many-body systems: Temporal entanglement and matrix-product state representation,” *Ann. Phys.* **435**, 168677 (2021), special issue on Philip W. Anderson.
- [19] E. Ye and G. K.-L. Chan, “Constructing tensor network influence functionals for general quantum dynamics,” *J. Chem. Phys.* **155**, 044104 (2021).
- [20] A. Foligno, T. Zhou, and B. Bertini, “Temporal entanglement in chaotic quantum circuits,” *Phys. Rev. X* **13**, 041008 (2023).
- [21] D. Perez-Garcia, F. Verstraete, M. M. Wolf, and J. I. Cirac, “Matrix product state representations,” *Quantum Info. Comput.* **7**, 401–430 (2007).
- [22] G. Vidal, “Efficient classical simulation of slightly entangled quantum computations,” *Phys. Rev. Lett.* **91**, 147902 (2003).
- [23] S. R. White and A. E. Feiguin, “Real-time evolution using the density matrix renormalization group,” *Phys. Rev. Lett.* **93**, 076401 (2004).
- [24] F. A. Pollock, C. Rodríguez-Rosario, T. Frauenheim, M. Paternostro, and K. Modi, “Non-markovian quantum processes: Complete framework and efficient characterization,” *Phys. Rev. A* **97**, 012127 (2018).
- [25] F. A. Pollock, C. Rodríguez-Rosario, T. Frauenheim, M. Paternostro, and K. Modi, “Operational markov condition for quantum processes,” *Phys. Rev. Lett.* **120**, 040405 (2018).
- [26] B. Bertini, P. Kos, and T. c. v. Prosen, “Exact correlation functions for dual-unitary lattice models in 1 + 1 dimensions,” *Phys. Rev. Lett.* **123**, 210601 (2019).
- [27] L. Piroli, B. Bertini, J. I. Cirac, and T. c. v. Prosen, “Exact dynamics in dual-unitary quantum circuits,” *Phys. Rev. B* **101**, 094304 (2020).
- [28] C. Jonay, V. Khemani, and M. Ippoliti, “Triunitary quantum circuits,” *Phys. Rev. Res.* **3**, 043046 (2021).
- [29] X.-H. Yu, Z. Wang, and P. Kos, “Hierarchical generalization of dual unitarity,” *Quantum* (2023), 10.22331/q-2024-02-20-1260.
- [30] B. Bertini, C. De Fazio, J. P. Garrahan, and K. Klobas, “Exact quench dynamics of the floquet quantum east model at the deterministic point,” *Phys. Rev. Lett.* **132**, 120402 (2024).
- [31] C. Liu and W. W. Ho, “Solvable entanglement dynamics in quantum circuits with generalized dual unitarity,” [arXiv:2312.12239](https://arxiv.org/abs/2312.12239).

- [32] A. Foligno, P. Kos, and B. Bertini, “Quantum information spreading in generalized dual-unitary circuits,” *Phys. Rev. Lett.* **132**, 250402 (2024).
- [33] K. Klobas, B. Bertini, and L. Piroli, “Exact thermalization dynamics in the “rule 54” quantum cellular automaton,” *Phys. Rev. Lett.* **126**, 160602 (2021).
- [34] A. Leroise, M. Sonner, and D. A. Abanin, “Scaling of temporal entanglement in proximity to integrability,” *Phys. Rev. B* **104**, 035137 (2021).
- [35] G. Giudice, G. Giudici, M. Sonner, J. Thoenniss, A. Leroise, D. A. Abanin, and L. Piroli, “Temporal entanglement, quasiparticles, and the role of interactions,” *Phys. Rev. Lett.* **128**, 220401 (2022).
- [36] J. Haegeman and F. Verstraete, “Diagonalizing transfer matrices and matrix product operators: A medley of exact and computational methods,” *Annu. Rev. Condens. Matter Phys.* **8**, 355 (2017).
- [37] We would like to draw a loose analogy between the relationship of zipper conditions and our solvable condition, with that of the Bethe ansatz and Yang-Baxter equations. The Bethe ansatz was initially proposed to solve exact eigenstates of the 1D Heisenberg spin chain, while Yang-Baxter equations capture the crucial point (factorizable scattering amplitudes) and the solutions give rise to a wide class of solvable models. Similarly, zipper conditions were used to solve specific models, while our solvable condition provides a systematic approach to constructing solvable quantum circuits.
- [38] See Supplemental Materials at [URL will be inserted by publisher] for derivations of the exact influence matrix, solvable two-site shift-invariant initial MPS, derivations of the Kraus-form representation for the boundary quantum channel, analytically calculating Rényi entropies dynamics for infinitely large subsystems, more details on the examples of $q = 2$, $\tilde{q} = 1$ and 2, and more details on the additional solvable condition, which further includes Refs. [70–75].
- [39] M. Piani, M. Horodecki, P. Horodecki, and R. Horodecki, “Properties of quantum nonsignaling boxes,” *Phys. Rev. A* **74**, 012305 (2006).
- [40] J. Kofler and i. c. v. Brukner, “Condition for macroscopic realism beyond the leggett-garg inequalities,” *Phys. Rev. A* **87**, 052115 (2013).
- [41] S. Milz, M. S. Kim, F. A. Pollock, and K. Modi, “Completely positive divisibility does not mean markovianity,” *Phys. Rev. Lett.* **123**, 040401 (2019).
- [42] Y.-Y. Hsieh, Z.-Y. Su, and H.-S. Goan, “Non-markovianity, information backflow, and system-environment correlation for open-quantum-system processes,” *Phys. Rev. A* **100**, 012120 (2019).
- [43] L. Li, M. J. Hall, and H. M. Wiseman, “Concepts of quantum non-markovianity: A hierarchy,” *Phys. Rep.* **759**, 1 (2018).
- [44] S. Milz and K. Modi, “Quantum stochastic processes and quantum non-markovian phenomena,” *PRX Quantum* **2**, 030201 (2021).
- [45] B. D. Anderson, “The realization problem for hidden markov models,” *Math. Control Signals Syst.* **12**, 80 (1999).
- [46] M. Vidyasagar, “The complete realization problem for hidden markov models: a survey and some new results,” *Math. Control Signals Syst.* **23**, 1 (2011).
- [47] M. Kliesch, D. Gross, and J. Eisert, “Matrix-product operators and states: Np-hardness and undecidability,” *Phys. Rev. Lett.* **113**, 160503 (2014).
- [48] This step can be traced back to the method of Markovian embedding, by incorporating additional degrees of freedom into the non-Markovian system to create the Markovian joint dynamics [76–87].
- [49] M. A. Nielsen and I. L. Chuang, *Quantum computation and quantum information* (Cambridge university press, 2010).
- [50] H.-P. Breuer, E.-M. Laine, J. Piilo, and B. Vacchini, “Colloquium: Non-markovian dynamics in open quantum systems,” *Rev. Mod. Phys.* **88**, 021002 (2016).
- [51] B. Bertini, K. Klobas, V. Alba, G. Lagnese, and P. Calabrese, “Growth of rényi entropies in interacting integrable models and the breakdown of the quasiparticle picture,” *Phys. Rev. X* **12**, 031016 (2022).
- [52] T. Zhou and A. W. Harrow, “Maximal entanglement velocity implies dual unitarity,” *Phys. Rev. B* **106**, L201104 (2022).
- [53] B. Bertini, P. Kos, and T. Prosen, “Operator entanglement in local quantum circuits ii: Solitons in chains of qubits,” *SciPost Phys.* **8**, 068 (2020).
- [54] M. Borsi and B. Pozsgay, “Construction and the ergodicity properties of dual unitary quantum circuits,” *Phys. Rev. B* **106**, 014302 (2022).
- [55] T. Prosen, “Many-body quantum chaos and dual-unitarity round-a-face,” *Chaos* **31** (2021), 10.1063/5.0056970.
- [56] R. Raussendorf and H. J. Briegel, “A one-way quantum computer,” *Phys. Rev. Lett.* **86**, 5188 (2001).
- [57] F. Verstraete and J. I. Cirac, “Valence-bond states for quantum computation,” *Phys. Rev. A* **70**, 060302 (2004).
- [58] P. W. Claeys, M. Henry, J. Vicary, and A. Lamacraft, “Exact dynamics in dual-unitary quantum circuits with projective measurements,” *Phys. Rev. Res.* **4**, 043212 (2022).
- [59] P. Kos and G. Styliaris, “Circuits of space and time quantum channels,” *Quantum* **7**, 1020 (2023).
- [60] P. W. Claeys, A. Lamacraft, and J. Vicary, “From dual-unitary to biunitary: a 2-categorical model for exactly-solvable many-body quantum dynamics,” *J. Phys. A: Math. Theor.* **57**, 335301 (2024).
- [61] R. Suzuki, K. Mitarai, and K. Fujii, “Computational power of one- and two-dimensional dual-unitary quantum circuits,” *Quantum* **6**, 631 (2022).
- [62] R. M. Milbradt, L. Scheller, C. Abmus, and C. B. Mendl, “Ternary unitary quantum lattice models and circuits in $2 + 1$ dimensions,” *Phys. Rev. Lett.* **130**, 090601 (2023).
- [63] B. Bertini, P. Kos, and T. c. v. Prosen, “Exact spectral form factor in a minimal model of many-body quantum chaos,” *Phys. Rev. Lett.* **121**, 264101 (2018).
- [64] B. Bertini and L. Piroli, “Scrambling in random unitary circuits: Exact results,” *Phys. Rev. B* **102**, 064305 (2020).
- [65] W. W. Ho and S. Choi, “Exact emergent quantum state designs from quantum chaotic dynamics,” *Phys. Rev. Lett.* **128**, 060601 (2022).
- [66] M. Ippoliti and W. W. Ho, “Dynamical purification and the emergence of quantum state designs from the projected ensemble,” *PRX Quantum* **4**, 030322 (2023).
- [67] E. B. Davies, “Markovian master equations,” *Communications in mathematical Physics* **39**, 91 (1974).
- [68] G. Lindblad, “On the generators of quantum dynamical semi-groups,” *Communications in Mathematical Physics* **48**, 119 (1976).
- [69] H.-P. Breuer and F. Petruccione, *The theory of open quantum systems* (Oxford University Press, UK, 2002).
- [70] F. Verstraete, J. J. Garcia-Ripoll, and J. I. Cirac, “Matrix product density operators: Simulation of finite-temperature and dissipative systems,” *Physical review letters* **93**, 207204 (2004).
- [71] G. D. las Cuevas, N. Schuch, D. Pérez-García, and J. I. Cirac, “Purifications of multipartite states: limitations and constructive methods,” *New J. Phys.* **15**, 123021 (2013).
- [72] N. Khaneja, R. Brockett, and S. J. Glaser, “Time optimal control in spin systems,” *Phys. Rev. A* **63**, 032308 (2001).

- [73] B. Kraus and J. I. Cirac, “Optimal creation of entanglement using a two-qubit gate,” *Phys. Rev. A* **63**, 062309 (2001).
- [74] J. Zhang, J. Vala, S. Sastry, and K. B. Whaley, “Geometric theory of nonlocal two-qubit operations,” *Phys. Rev. A* **67**, 042313 (2003).
- [75] S. Aravinda, S. A. Rather, and A. Lakshminarayan, “From dual-unitary to quantum bernoulli circuits: Role of the entangling power in constructing a quantum ergodic hierarchy,” *Phys. Rev. Res.* **3**, 043034 (2021).
- [76] A. Imamoglu, “Stochastic wave-function approach to non-markovian systems,” *Phys. Rev. A* **50**, 3650 (1994).
- [77] B. M. Garraway, “Nonperturbative decay of an atomic system in a cavity,” *Phys. Rev. A* **55**, 2290 (1997).
- [78] L. Mazzola, S. Maniscalco, J. Piilo, K.-A. Suominen, and B. M. Garraway, “Pseudomodes as an effective description of memory: Non-markovian dynamics of two-state systems in structured reservoirs,” *Phys. Rev. A* **80**, 012104 (2009).
- [79] J. Iles-Smith, N. Lambert, and A. Nazir, “Environmental dynamics, correlations, and the emergence of noncanonical equilibrium states in open quantum systems,” *Phys. Rev. A* **90**, 032114 (2014).
- [80] S. Kretschmer, K. Luoma, and W. T. Strunz, “Collision model for non-markovian quantum dynamics,” *Phys. Rev. A* **94**, 012106 (2016).
- [81] S. Campbell, F. Ciccarello, G. M. Palma, and B. Vacchini, “System-environment correlations and markovian embedding of quantum non-markovian dynamics,” *Phys. Rev. A* **98**, 012142 (2018).
- [82] D. Tamascelli, A. Smirne, S. F. Huelga, and M. B. Plenio, “Nonperturbative treatment of non-markovian dynamics of open quantum systems,” *Phys. Rev. Lett.* **120**, 030402 (2018).
- [83] I. A. Luchnikov, S. V. Vintskevich, H. Ouerdane, and S. N. Filippov, “Simulation complexity of open quantum dynamics: Connection with tensor networks,” *Phys. Rev. Lett.* **122**, 160401 (2019).
- [84] F. Mascherpa, A. Smirne, A. D. Somoza, P. Fernández-Acebal, S. Donadi, D. Tamascelli, S. F. Huelga, and M. B. Plenio, “Optimized auxiliary oscillators for the simulation of general open quantum systems,” *Phys. Rev. A* **101**, 052108 (2020).
- [85] I. A. Luchnikov, S. V. Vintskevich, D. A. Grigoriev, and S. N. Filippov, “Machine learning non-markovian quantum dynamics,” *Phys. Rev. Lett.* **124**, 140502 (2020).
- [86] S. N. Filippov and I. A. Luchnikov, “Collisional open quantum dynamics with a generally correlated environment: Exact solvability in tensor networks,” *Phys. Rev. A* **105**, 062410 (2022).
- [87] S. Flannigan, F. Damanet, and A. J. Daley, “Many-body quantum state diffusion for non-markovian dynamics in strongly interacting systems,” *Phys. Rev. Lett.* **128**, 063601 (2022).

Supplementary Materials for: Exact Hidden Markovian Dynamics in Quantum Circuits

He-Ran Wang,¹ Xiao-Yang Yang,^{1,2} and Zhong Wang^{1,*}

¹Institute for Advanced Study, Tsinghua University, Beijing 100084, People's Republic of China

²Department of Physics, Tsinghua University, Beijing 100084, People's Republic of China

I. EXACT INFLUENCE MATRIX FROM THE SOLVABLE CONDITION

In this section, we derive the exact influence matrix in the Matrix Product State (MPS) representation from the solvable condition. We present the proof from two directions: First, we perform straightforward contractions on the 1+1D tensor network to obtain the influence matrix on the time slice (Sec. IA); Second, we show that the obtained influence matrix is indeed the fixed point of the spatial transfer matrix (Sec. IB). All the calculations are shown in diagrammatic representations.

A. Contractions of the tensor network

We summarize the procedure of contractions in Fig. S1. We begin with the tensor network representing the traced time-evolved state in the region L, as depicted in Fig. S1(a) [see also Fig. 1(b) in the main text]. In the first step, we apply the following two local rules: the unitarity of local gates

$$\begin{array}{c} \circ \\ \diagup \quad \diagdown \\ \square \\ \diagdown \quad \diagup \\ \circ \end{array} = \begin{array}{c} \circ \\ | \\ \circ \end{array} \quad , \quad (S1)$$

and the left-canonical condition of the MPS

$$\begin{array}{c} \circ \\ | \\ \square \\ | \\ \bullet \end{array} = \begin{array}{c} \bullet \\ | \\ \bullet \end{array} . \quad (S2)$$

The two local rules allow efficient contractions of the tensor network within the lightcone. More specifically, all the tensors in the space-time region $2t - x > 2T$ are reduced to the identities lying along the edge of the lightcone $2t - x = 2T$, as shown in Fig. S1(b). Notice that this step is independent of the solvable condition, and thus is universal for brickwork quantum circuits.

Next, we employ the solvable condition to achieve further simplifications:

$$\begin{array}{c} \circ \\ | \\ \square \\ | \\ \square \end{array} = \begin{array}{c} \circ \\ \diagdown \quad \diagup \\ \square \\ \diagup \quad \diagdown \\ \square \end{array} = \begin{array}{c} \square \\ | \\ \square \end{array} . \quad (S3)$$

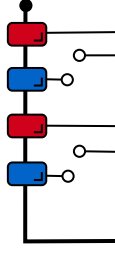
For instance, we can apply this condition on the tensor located at the lower-left corner in Fig. S1(b) (circled by the grey dotted line), which gives

$$\begin{array}{c} \circ \\ \diagdown \quad \diagup \\ \square \\ \diagup \quad \diagdown \\ \square \end{array} = \begin{array}{c} \square \\ \diagdown \quad \diagup \\ \square \end{array} . \quad (S4)$$

We perform such contractions along the edge of the lightcone $2t - x = 2T$ to shift the identities to the next edge, as shown in Fig. S1 (c). By repeating this “lightcone decimation” procedure for T times, we arrive at the closed-form influence matrix with outer legs across the time slice, the same as Fig. 1(c) in the main text.

The contractions imply a novel manifestation of *space-time duality* between the initial state MPS and the influence matrix: The local MPS located at an even site x in the initial state exactly corresponds to the local MPS in the influence matrix at $t = -x/2$.

Notice that the solvable condition Eq. (S3) we imposed is irrelevant of the tensor B . Following the same approach presented in Fig. S1, one can show that tracing out the left region results in the following influence matrix (an example for $t = 2$):

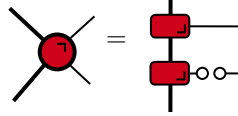


(S9)

II. BOUNDARY QUANTUM CHANNEL

A. Kraus-operator representation

In this subsection, we derive the concrete expressions of the time-local boundary quantum channel defined by



(S10)

The action of quantum channel can be directly read out from the diagram following the down-to-up direction:

$$\mathcal{M}(\tilde{\rho}_R) = \sum_{b,b'=0}^{q-1} A^{(b)} \left(\sum_{a=0}^{q-1} A^{(a)} \text{Tr}_{x=0}[\tilde{\rho}_R] A^{(a)\dagger} \right) A^{(b')\dagger} \otimes (|b\rangle\langle b'|)_{x=0}. \quad (\text{S11})$$

We shall bring this expression into the standard Kraus representation. To this end, we rewrite the trace operation over the Hilbert space at $x = 0$ as $\text{Tr}_{x=0}[\tilde{\rho}_R] = \sum_{a'=0}^{q-1} \langle a' | \tilde{\rho}_R | a' \rangle$. Plugging this decomposition into Eq. (S11) leads to

$$\mathcal{M}(\tilde{\rho}_R) = \sum_{a,a',b,b'=0}^{q-1} [A^{(b)} A^{(a)} \otimes (|b\rangle\langle a'|)_{x=0}] \tilde{\rho}_R [A^{(a)\dagger} A^{(b')\dagger} \otimes (|a'\rangle\langle b'|)_{x=0}]. \quad (\text{S12})$$

The summation is over a, a', b, b' . However, notice that the index b and b' appear in different sides of $\tilde{\rho}_R$ independently. Therefore, we can recast the operators on the single side of $\tilde{\rho}_R$ into the Kraus operator by summing over b :

$$K_{a,a'} = \sum_{b=0}^{q-1} A^{(b)} A^{(a)} \otimes (|b\rangle\langle a'|)_{x=0}. \quad (\text{S13})$$

Consequently, Eq. (S11) becomes $\mathcal{M}(\tilde{\rho}_R) = \sum_{a,a'=0}^{q-1} K_{a,a'} \tilde{\rho}_R K_{a,a'}^\dagger$. We can check the trace-preserving property of Kraus operators as follows:

$$\begin{aligned} \sum_{a,a'=0}^{q-1} K_{a,a'}^\dagger K_{a,a'} &= \sum_{a,a',b,b'=0}^{q-1} A^{(a)\dagger} A^{(b)\dagger} A^{(b')} A^{(a)} \otimes |a'\rangle\langle b| b'\rangle\langle a'| \\ &= \left(\sum_{a,b,b'=0}^{q-1} \delta_{b,b'} A^{(a)\dagger} A^{(b)\dagger} A^{(b')} A^{(a)} \right) \otimes \left(\sum_{a'=0}^{q-1} |a'\rangle\langle a'| \right) \\ &= \sum_{a=0}^{q-1} A^{(a)\dagger} \left(\sum_{b=0}^{q-1} A^{(b)\dagger} A^{(b)} \right) A^{(a)} \otimes I_q \\ &= \sum_{a=0}^{q-1} A^{(a)\dagger} A^{(a)} \otimes I_q = I_\chi \otimes I_q. \end{aligned} \quad (\text{S14})$$

Here the equation $\sum_{a=0}^{q-1} A^{(a)\dagger} A^{(a)} = I_\chi$ comes from the left-canonical condition.

Similarly, for the case of two-site shift invariant initial MPS described in Sec. IC, the Kraus operators are given by

$$K_{a,a'} = \sum_{b=0}^{q-1} A^{(b)} B^{(a)} \otimes (|b\rangle \langle a'|)_{x=0}. \quad (\text{S15})$$

B. Mixed initial states

Here, we generalize the quantum channel expression to the mixed initial states admitting Matrix Product Density Operator (MPDO) representation. We further impose the locally purified condition, that is, the MPDO can be purified to a MPS with a local purifying auxiliary system [5, 6]. MPDO with the locally purified condition is also termed as the Locally Purified Density Operator (LPDO). In this case, the three-leg local tensor \mathcal{A} reads

$$j, j' \text{ --- } \boxed{\text{red}} \text{ --- } k, k' = \mathcal{A}_{jk, j'k'}^{(a, a')} = \sum_{\gamma=0}^{D-1} A_{jk}^{(a, \gamma)} A_{j'k'}^{(a', \gamma)*}, \quad (\text{S16})$$

where γ is the auxiliary index corresponding to the local purification space of dimension D . In this context, the left-canonical condition is formulated as

$$\sum_{\gamma=0}^{D-1} \sum_{a=0}^{q-1} A^{(a, \gamma)\dagger} A^{(a, \gamma)} = I_\chi. \quad (\text{S17})$$

For the $D = 1$ case, the LPDO is reduced to the pure-state MPS studied in the main text.

The LPDO corresponds to the quantum channel

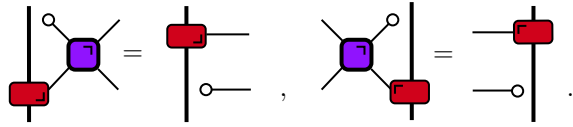
$$\mathcal{M}(\tilde{\rho}_R) = \sum_{\gamma'=0}^{D-1} \sum_{b, b'=0}^{q-1} A^{(b, \gamma')} \left(\sum_{\gamma=0}^{D-1} \sum_{a=0}^{q-1} A^{(a, \gamma)} \text{Tr}_{x=0}[\tilde{\rho}_R] A^{(a, \gamma)\dagger} \right) A^{(b', \gamma')\dagger} \otimes (|b\rangle \langle b'|)_{x=0}. \quad (\text{S18})$$

Following the similar analysis, we can extract the Kraus operators from the quantum channel expression:

$$K_{(a\gamma, a'\gamma')} = \sum_{b=0}^{q-1} A^{(b, \gamma')} A^{(a, \gamma)} \otimes (|b\rangle \langle a'|)_{x=0}. \quad (\text{S19})$$

III. RÉNYI ENTROPIES DYNAMICS

Here, we perform tensor-network contractions to obtain analytical expressions for the time-evolved Rényi entropies $S_R^{(n)}(t) = \ln(\text{Tr}[\rho_R^n(t)])/(1-n)$, where $n \in \mathbb{Z}$ and $n > 1$. We work in the space-time regime where size(L) and size(R) are larger than $2t$, such that the most efficient contractions of tensor networks from both sides are allowed. This regime corresponds to the early-stage growth of entanglement. Due to the presence of the strict light cone in brickwork architectures, we can extend size(L) and size(R) to be infinite, without altering the results. As demonstrated in the main text, we impose two solvable conditions with opposite chirality, quoted as below:



$$(\text{S20})$$

Meanwhile, we choose the initial state as the homogeneous, one-site shift invariant MPS with local tensor A . To dispense with the influence of boundary conditions, we further assume that the MPS is in the left- and right-canonical form: $\sum_{a=0}^{q-1} A^{(a)\dagger} A^{(a)} = \sum_{a=0}^{q-1} A^{(a)} A^{(a)\dagger} = I_\chi$.

In Sec. III A, we introduce basic notations of the multi-folded representation, which are demanded to present $\text{Tr}[\rho_R^n(t)]$ graphically. Subsequently, we apply the solvable conditions to contract the tensor network in Sec. III B, and establish the

Therefore, we have:

$$\text{Tr}[\rho_R^n(t)] = \text{Diagram} \quad (\text{S25})$$

B. Entanglement velocity

In this subsection, we show that the tensor network in Eq. (S25) can be efficiently contracted utilizing the two solvable conditions. The crucial point is to establish the contraction rules in the n -folded representation. First, notice that the time-unitarity condition leads to the following two rules:

$$\text{Diagram 1} = \text{Diagram 2}, \quad \text{Diagram 3} = \text{Diagram 4} \quad (\text{S26})$$

The two contraction rules can be verified by noticing that both two kinds of pairing operators couple between U and U^* . The unitarity together with left- and right-canonical property of the MPS allow contractions of the tensor network within the lightcone:

$$\text{Tr}[\rho_R^n(t)] = \text{Diagram} \quad (\text{S27})$$

Second, and most importantly, notice that the solvable conditions can be represented in the n -folded picture exactly the same as those in the folded picture [Eq. (S20)]:

$$\text{Diagram 1} = \text{Diagram 2}, \quad \text{Diagram 3} = \text{Diagram 4} \quad (\text{S28})$$

Consequently, we obtain a highly simplified graphical representation:

$$\text{Tr}[\rho_R^n(t)] = \text{Diagram} = \text{Diagram} \quad (\text{S29})$$

The resulting one-dimensional tensor network can be demonstrated as the consecutive action of a two-site transfer matrix \mathbb{T} with appropriate initial and final states. Here \mathbb{T} acts on $2n$ -replica Hilbert space, defined as

$$\mathbb{T} = \text{Diagram} \quad (\text{S30})$$

A. Preliminary: two-qubit gates

To begin with, notice that every two-qubit unitary gate can be parameterized as [11–13]:

$$U = e^{i\phi}(u_+ \otimes u_-)V[J_1, J_2, J_3](v_- \otimes v_+), \quad (\text{S37})$$

where $u_{\pm}, v_{\pm} \in \text{SU}(2)$, and

$$V[J_1, J_2, J_3] = \exp[-i(J_1\sigma^1 \otimes \sigma^1 + J_2\sigma^2 \otimes \sigma^2 + J_3\sigma^3 \otimes \sigma^3)]. \quad (\text{S38})$$

Since increasing any J_{α} by $\frac{\pi}{2}$ is equivalent to applying a tensor product of two single-site unitaries which can be absorbed into u_{\pm}, v_{\pm} , we can restrict the range of J_{α} within $[0, \frac{\pi}{2})$. The matrix $V[J_1, J_2, J_3]$ can also be written on the Pauli basis [10]:

$$V[J_1, J_2, J_3] = \sum_{\alpha=0}^3 V_{\alpha}(J_1, J_2, J_3)\sigma^{\alpha} \otimes \sigma^{\alpha}, \quad (\text{S39})$$

where the identity has been included in the Pauli matrices as $\sigma^0 = I_2$. Here $V_{\alpha}(J_1, J_2, J_3)$ are some complex-valued coefficients:

$$\begin{aligned} V_0(J_1, J_2, J_3) &= \cos(J_1) \cos(J_2) \cos(J_3) - i \sin(J_1) \sin(J_2) \sin(J_3), \\ V_1(J_1, J_2, J_3) &= \cos(J_1) \sin(J_2) \sin(J_3) - i \sin(J_1) \cos(J_2) \cos(J_3), \\ V_2(J_1, J_2, J_3) &= \sin(J_1) \cos(J_2) \sin(J_3) - i \cos(J_1) \sin(J_2) \cos(J_3), \\ V_3(J_1, J_2, J_3) &= \sin(J_1) \sin(J_2) \cos(J_3) - i \cos(J_1) \cos(J_2) \sin(J_3). \end{aligned} \quad (\text{S40})$$

We adopt this parameterization and identify the constraints on all the parameters (u_{\pm}, v_{\pm} and $J_{1,2,3}$) under the solvable condition.

B. $q = 2, \tilde{q} = 1$

Here we choose the one-site state to be $|0\rangle$, that is, $\mathcal{H}_A = |0\rangle\langle 0|$. The solvable condition reads $U^R(|0\rangle\langle 0| \otimes I_2)(U^R)^{\dagger} = I_2 \otimes |0\rangle\langle 0|$, where U^R represents the reshuffled operator of U as defined in the main text.

In terms of Eq. (S37), the solvable condition can be rewritten as

$$V^R[J_1, J_2, J_3][(v_- |0\rangle\langle 0| v_-^{\dagger}) \otimes I_2](V^R[J_1, J_2, J_3])^{\dagger} = I_2 \otimes (u_-^{\dagger} |0\rangle\langle 0| u_-). \quad (\text{S41})$$

We consider a *necessary condition* for this equation by partially tracing out the first site degrees of freedom in this equation. To perform the trace operation, a trick is to rewrite the matrix $V[J_1, J_2, J_3]$ as

$$V[J_1, J_2, J_3] = V[J'_1, J'_2, J'_3]V[\frac{\pi}{4}, \frac{\pi}{4}, \frac{\pi}{4}], \quad (\text{S42})$$

where $V[\frac{\pi}{4}, \frac{\pi}{4}, \frac{\pi}{4}]$ is the SWAP gate exchanging the states of two qubits, $J'_{\alpha} = J_{\alpha} - \frac{\pi}{4}$, $-\frac{\pi}{4} \leq J'_{\alpha} < \frac{\pi}{4}$. From now on, we will abbreviate the coefficients $V_{\alpha}(J'_1, J'_2, J'_3)$ to V'_{α} . Next, we apply the partial trace on Eq. (S41) and write it in the time direction:

$$\text{Tr}_l\{V[J'_1, J'_2, J'_3][I_2 \otimes (v_- |0\rangle\langle 0| v_-^{\dagger})]V^{\dagger}[J'_1, J'_2, J'_3]\} = 2u_-^{\dagger} |0\rangle\langle 0| u_-. \quad (\text{S43})$$

We can calculate this equation by expanding the expression in the curly brackets on the Pauli basis of the left site, followed by the trace operation. It leaves

$$\sum_{\alpha=0}^3 |V'_{\alpha}|^2 (\sigma^{\alpha} v_- |0\rangle\langle 0| v_-^{\dagger} \sigma^{\alpha}) = u_-^{\dagger} |0\rangle\langle 0| u_-. \quad (\text{S44})$$

The left hand side is the summation of four rank-1 projectors with positive semi-definite coefficients, while on the right hand side there is one rank-1 projector. The equality holds only when the projector $u_-^{\dagger} |0\rangle\langle 0| u_-$ is exactly the same as those projectors $\sigma^{\alpha} v_- |0\rangle\langle 0| v_-^{\dagger} \sigma^{\alpha}$ with non-zero coefficients $|V'_{\alpha}|^2$.

We now show that it is impossible that three or all of V'_{α} are non-zero. Consider the case that V'_{α} and V'_{β} are non-zero, and thus $\sigma^{\alpha} v_- |0\rangle$ and $\sigma^{\beta} v_- |0\rangle$ are the same as $u_-^{\dagger} |0\rangle$ up to a phase factor, $\alpha \neq \beta$. We can directly deduce that $v_- |0\rangle$ is an eigenstate of $\sigma^{\alpha} \sigma^{\beta}$. If there is another non-zero coefficient V'_{γ} , $v_- |0\rangle$ should be an eigenstate of $\sigma^{\beta} \sigma^{\gamma}$, which is impossible because

$[\sigma^\alpha \sigma^\beta, \sigma^\beta \sigma^\gamma] \neq 0$. Therefore, the three coefficients $V'_{\alpha,\beta,\gamma}$ can not simultaneously be non-zero. Meanwhile, due to range of parameters $-\frac{\pi}{4} \leq J'_\alpha < \frac{\pi}{4}$, V'_0 can never be zero. Hence, we only need to consider the following two classes:

- (1) V'_0 and one of $V'_{\alpha \neq 0}$ are non-zero;
- (2) Only V'_0 is non-zero.

We start from the first class and take $\alpha = 3$ for instance. It follows that $v_- |0\rangle$ and $u_-^\dagger |0\rangle$ are eigenstates of σ^3 with the same eigenvalue. We can therefore parameterize the single-site special unitaries as: (I) $v_- = e^{-i\eta\sigma^3}$, $u_- = e^{-i\epsilon\sigma^3}$, or (II) $v_- = i\sigma^1 e^{-i\eta\sigma^3}$, $u_- = ie^{-i\epsilon\sigma^3} \sigma^1$. As for the coefficients, we have

$$|V'_0|^2 + |V'_3|^2 = 1, V'_1 = V'_2 = 0, \quad (\text{S45})$$

of which the only solution is $J'_1 = J'_2 = 0$. It can be checked that this solution combined with (I) fulfill the original solvable condition Eq. (S41). This results in the set of unitary gates parameterized as Eq. (11) in the main text:

$$\begin{aligned} U &= e^{i\phi}(u_+ \otimes e^{-i\epsilon\sigma^3})V[0, 0, J'_3]V[\frac{\pi}{4}, \frac{\pi}{4}, \frac{\pi}{4}](e^{-i\eta\sigma^3} \otimes v_+) \\ &= e^{i\phi}(u_+ \otimes e^{-i\epsilon\sigma^3})V[\frac{\pi}{4}, \frac{\pi}{4}, J_3](e^{-i\eta\sigma^3} \otimes v_+). \end{aligned} \quad (\text{S46})$$

On the other hand, the single-site unitaries (II) can be included into Eq. (S46) through the following transformation:

$$\begin{aligned} U &= e^{i\phi}[u_+ \otimes (ie^{-i\epsilon\sigma^3} \sigma^1)]V[\frac{\pi}{4}, \frac{\pi}{4}, J_3][(i\sigma^1 e^{-i\eta\sigma^3}) \otimes v_+] \\ &= e^{i\phi}[(iu_+ \sigma^1) \otimes e^{-i\epsilon\sigma^3}]V[\frac{\pi}{4}, \frac{\pi}{4}, J_3][e^{-i\eta\sigma^3} \otimes (i\sigma^1 v_+)]. \end{aligned} \quad (\text{S47})$$

Other cases in the first class ($\alpha = 1$ or 2) can be analyzed following a similar approach. It turns out that all the solutions are covered by Eq. (S46).

Next, we consider the second class, where $V'_1 = V'_2 = V'_3 = 0$. This condition leads to $J'_\alpha = 0$, and $v_- u_- = e^{i\alpha}$. The solutions read

$$U = e^{i\phi}(u_+ \otimes u_-)V[\frac{\pi}{4}, \frac{\pi}{4}, \frac{\pi}{4}](v_- \otimes v_+) = e^{i(\phi+\alpha)}(u_+ \otimes I_2)V[\frac{\pi}{4}, \frac{\pi}{4}, \frac{\pi}{4}](I_2 \otimes v_+), \quad (\text{S48})$$

which, again, are covered by Eq. (S46).

To conclude, we have exhausted the two-qubit gates fulfilling the solvable condition for $\tilde{q} = 1$. We obtain the solutions Eq. (S46) by rigorously classifying and discussing the consequences of a *necessary condition* Eq. (S43), while the solutions can be verified to fulfill the *sufficient condition*. We point out that all the gates given by Eq. (S43) are dual-unitary gates [9]. Remarkably, the solutions coincide with those two-qubit circuits characterized by chiral solitons [10], defined by the soliton condition: $U^\dagger(\sigma^3 \otimes I)U = I \otimes \sigma^3$.

C. $q = 2, \tilde{q} = 2$

In this subsection we consider $\tilde{q} = 2$ where $\mathcal{H}_A = \mathcal{H}_{q=2}$. Notice that solutions for $\tilde{q} = 2$ must form a subset of solutions for $\tilde{q} = 1$. Therefore, we can apply the $\tilde{q} = 2$ solvable condition on $\tilde{q} = 1$ solutions to further restrict the parameters. It follows that

$$V^R[\frac{\pi}{4}, \frac{\pi}{4}, J_3](e^{-i\eta\sigma^3} \rho e^{i\eta\sigma^3} \otimes I_2)(V^R[\frac{\pi}{4}, \frac{\pi}{4}, J_3])^\dagger = I_2 \otimes e^{i\epsilon\sigma^3} \rho e^{-i\epsilon\sigma^3}, \quad (\text{S49})$$

which holds for arbitrary one-site operator ρ .

We consider a sufficient condition by partially tracing out the first site degrees of freedom, and expand the matrix V on the Pauli basis, which gives:

$$\cos^2(J'_3)(e^{-i(\eta+\epsilon)\sigma^3} \rho e^{i(\eta+\epsilon)\sigma^3}) + \sin^2(J'_3)(\sigma^3 e^{-i(\eta+\epsilon)\sigma^3} \rho e^{i(\eta+\epsilon)\sigma^3} \sigma^3) = \rho. \quad (\text{S50})$$

The left hand side could be viewed as a quantum channel with two Kraus operators: $K_0 = \cos(J'_3)e^{-i(\eta+\epsilon)\sigma^3}$, $K_1 = \sin(J'_3)\sigma^3 e^{-i(\eta+\epsilon)\sigma^3}$. In this context, Eq. (S50) states that the quantum channel should be an identity operation, which requires that $J'_3 = 0, \eta + \epsilon = 0$. The corresponding gates are

$$U = e^{i\phi}(u \otimes I_2)S, \quad (\text{S51})$$

where $S = V[\frac{\pi}{4}, \frac{\pi}{4}, \frac{\pi}{4}]$ is the SWAP gate. It can be checked that all the gates in the form of Eq. (S51) fulfill the $\tilde{q} = 2$ solvable condition.

V. SOLVABLE CONDITIONS WITH OPPOSITE CHIRALITY

In this section, we discuss the relationship between two solvable conditions with opposite chirality [Eq. (S20)]. We also present several examples that simultaneously fulfill both solvable conditions, allowing for exact calculations of Rényi entropy dynamics, as demonstrated in Sec. III.

First of all, we establish a one-to-one correspondence between the solutions of two solvable conditions. To be concrete, given the three-leg tensor $A_{jk}^{(a)}$ as input, the solvable condition Eq. (S3) can be expressed as

$$U^R(|A_{jk}\rangle\langle A_{j'k'}| \otimes I_q)(U^R)^\dagger = I_q \otimes |A_{jk}\rangle\langle A_{j'k'}|. \quad (\text{S52})$$

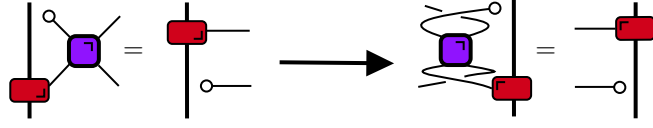
We show that $U_S = SUS$ (S is the SWAP gate) must satisfy the opposite-chirality solvable condition. We denote the reshuffled operator of U_S as U_S^R , and express the opposite-chirality solvable condition in the space direction from right to left, which involves the action of $(U_S^R)^T$ as:

$$(U_S^R)^T(|A_{jk}\rangle\langle A_{j'k'}| \otimes I_q)(U_S^R)^* = U_R(|A_{jk}\rangle\langle A_{j'k'}| \otimes I_q)(U_R)^\dagger = I_q \otimes |A_{jk}\rangle\langle A_{j'k'}|. \quad (\text{S53})$$

Here, we have utilized the transformation $(U_S^R)^T = U^R$, which can be proven as follows [14]:

$$[(U_S^R)^T]_{ab}^{cd} = (U_S^R)_{cd}^{ab} = (SUS)_{ca}^{db} = U_{bd}^{ac} = (U^R)_{ab}^{cd}. \quad (\text{S54})$$

We illustrate the above analysis in the following diagrammatic representation:



$$(\text{S55})$$

The reverse holds as well: a solution of the solvable condition with single-site MPS on the right can be mapped to the left solution by applying the SWAP gate.

For $q = 2, \tilde{q} = 1$, we have exhausted the solutions fulfilling one-sided solvable condition as solved in Eq. (S46):

$$U_+ = e^{i\phi}(u_+ \otimes e^{-i\epsilon\sigma^3})V[\frac{\pi}{4}, \frac{\pi}{4}, J_3](e^{-i\eta\sigma^3} \otimes v_+). \quad (\text{S56})$$

The subscript $+$ represents the chirality of the solvable condition. Using the correspondence introduced above, we can directly present the solutions for the opposite-chirality solvable condition as:

$$U_- = e^{i\phi}(e^{-i\epsilon'\sigma^3} \otimes u_-)V[\frac{\pi}{4}, \frac{\pi}{4}, J_3](v_- \otimes e^{-i\eta'\sigma^3}). \quad (\text{S57})$$

Consequently, we can obtain the exhaustive parameterization for two-qubit gates fulfilling both solvable conditions by examining the overlap of two sets of solutions, which gives:

$$U = e^{i\phi}(e^{-i\epsilon'\sigma^3} \otimes e^{-i\epsilon\sigma^3})V[\frac{\pi}{4}, \frac{\pi}{4}, J_3](e^{-i\eta\sigma^3} \otimes e^{-i\eta'\sigma^3}). \quad (\text{S58})$$

For $q = 4, \tilde{q} = 2$, we have presented a subclass of solutions as Eq. (12) of the main text: $U_+ = e^{i\phi}W_2SW_1(I \otimes v_+)$, where $v_+ \in \text{SU}(4)$, $W_{1,2} = \sum_{a=0}^3 f_{1,2}^{(a)} \otimes |a\rangle\langle a|$, $f_1^{(a)} = \begin{pmatrix} I_2 & 0 \\ 0 & g^{(a)} \end{pmatrix}$, $g^{(a)} \in \text{SU}(2)$, and $f_2^{(a)} \in \text{SU}(4)$ for all a . The corresponding opposite-chirality solutions can be parameterized as $U_- = e^{i\phi}SW_2SW_1S(v_- \otimes I)$. The overlap of these two sets of solutions gives

$$U = e^{i\phi}(u_+ \otimes u_-)S \exp(-iH)(v_- \otimes v_+), \quad (\text{S59})$$

where H is a real symmetric matrix $H \in \mathbb{R}^q \times \mathbb{R}^q$, $H_{ab} = 0$ for $a = 0, 1$ or $b = 0, 1$, and u_{\pm}, v_{\pm} take the direct sum form as $\begin{pmatrix} I_2 & 0 \\ 0 & w \end{pmatrix}$, $w \in \text{SU}(2)$.

* wangzhongemail@tsinghua.edu.cn

- [1] M. C. Bañuls, M. B. Hastings, F. Verstraete, and J. I. Cirac, “Matrix product states for dynamical simulation of infinite chains,” *Phys. Rev. Lett.* **102**, 240603 (2009).
- [2] A. Müller-Hermes, J. I. Cirac, and M. C. Bañuls, “Tensor network techniques for the computation of dynamical observables in one-dimensional quantum spin systems,” *New J. Phys.* **14**, 075003 (2012).
- [3] M. B. Hastings and R. Mahajan, “Connecting entanglement in time and space: Improving the folding algorithm,” *Phys. Rev. A* **91**, 032306 (2015).
- [4] A. Lerose, M. Sonner, and D. A. Abanin, “Influence matrix approach to many-body floquet dynamics,” *Phys. Rev. X* **11**, 021040 (2021).
- [5] F. Verstraete, J. J. Garcia-Ripoll, and J. I. Cirac, “Matrix product density operators: Simulation of finite-temperature and dissipative systems,” *Physical review letters* **93**, 207204 (2004).
- [6] G. D. las Cuevas, N. Schuch, D. Pérez-García, and J. I. Cirac, “Purifications of multipartite states: limitations and constructive methods,” *New J. Phys.* **15**, 123021 (2013).
- [7] B. Bertini, C. De Fazio, J. P. Garrahan, and K. Klobas, “Exact quench dynamics of the floquet quantum east model at the deterministic point,” *Phys. Rev. Lett.* **132**, 120402 (2024).
- [8] B. Bertini and L. Piroli, “Scrambling in random unitary circuits: Exact results,” *Phys. Rev. B* **102**, 064305 (2020).
- [9] B. Bertini, P. Kos, and T. c. v. Prosen, “Exact correlation functions for dual-unitary lattice models in $1 + 1$ dimensions,” *Phys. Rev. Lett.* **123**, 210601 (2019).
- [10] B. Bertini, P. Kos, and T. Prosen, “Operator entanglement in local quantum circuits ii: Solitons in chains of qubits,” *SciPost Phys.* **8**, 068 (2020).
- [11] N. Khaneja, R. Brockett, and S. J. Glaser, “Time optimal control in spin systems,” *Phys. Rev. A* **63**, 032308 (2001).
- [12] B. Kraus and J. I. Cirac, “Optimal creation of entanglement using a two-qubit gate,” *Phys. Rev. A* **63**, 062309 (2001).
- [13] J. Zhang, J. Vala, S. Sastry, and K. B. Whaley, “Geometric theory of nonlocal two-qubit operations,” *Phys. Rev. A* **67**, 042313 (2003).
- [14] S. Aravinda, S. A. Rather, and A. Lakshminarayan, “From dual-unitary to quantum bernoulli circuits: Role of the entangling power in constructing a quantum ergodic hierarchy,” *Phys. Rev. Res.* **3**, 043034 (2021).